THE JOURNAL OF PHYSICAL CHEMISTRY B

Article

pubs.acs.org/JPCB

Aqueous Suspensions of $GdPO_4$ Nanorods: A Paramagnetic Mineral Liquid Crystal

Benjamin Abécassis,*[,†] Frédéric Lerouge,[‡] Frédéric Bouquet,[†] Souad Kachbi,[§] Maelle Monteil,[§] and Patrick Davidson[†]

[†]Laboratoire de Physique des Solides, Univ. Paris-Sud, CNRS, UMR 8502, F-91405 Orsay Cedex, France

[‡]Laboratoire de Chimie, Université Lyon 1, ENS Lyon, CNRS, UMR 5182, F-69364 Lyon 07, France

[§]Laboratory CSPBAT, Université Paris 13, UMR 7244 CNRS, F-93017 Bobigny, France

Supporting Information

ABSTRACT: Colloidal suspensions of rod-like nanoparticles are well-known to readily form liquid-crystalline phases. Using mineral nanoparticles for this purpose may impart their liquid-crystalline suspensions with original physical properties. We synthesized $GdPO_4$ nanorods whose aqueous suspensions spontaneously organize in a nematic phase at high concentrations. The nematic phase is very well aligned by small magnetic fields, and the isotropic phase displays a very large field-induced birefringence. Moreover, the nanorods migrate to regions of high magnetic field. On the basis of magnetization measurements, we show that this unusual behavior is due to the fact that $GdPO_4$ nanorods are actually paramagnetic. Such a paramagnetic mineral liquid crystal, easily synthesized and little sensitive to temperature, may be an interesting alternative to organometallic thermotropic liquid crystals for applications where magnetic field alignment would be more suitable than electric field alignment.

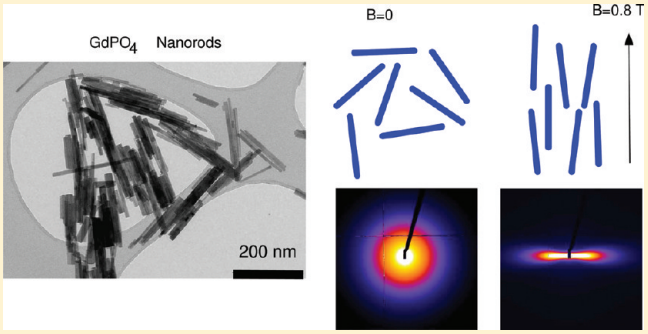

INTRODUCTION

Depending on concentration, colloidal suspensions of anisotropic nanoparticles are well-known to spontaneously form liquid-crystalline phases.[1] This behavior is now fairly well understood both from theoretical arguments and from numerical simulations.[2−4] Indeed, liquid-crystalline ordering of suspensions was already observed whatever the precise chemical nature of the anisotropic nanoparticles, namely, organic or mineral, natural or synthetic.[5,6] The most common and important liquid-crystalline phases, that is, nematic, lamellar, and columnar phases, have now been discovered in these systems, in good agreement with theory and simulations. However, there are still a number of open issues that require more attention such as the influence of polydispersity and particle chirality, the role of electrostatic interactions in aqueous suspensions, and the onset of one-dimensional or two-dimensional positional order.[7,8] From another point of view, one interest of considering colloidal suspensions of mineral nanoparticles is that mineral building blocks may impart interesting physical properties to their liquid-crystalline assemblies. For example, there have been so far several reports of nematic suspensions of nanoparticles that have unusual magnetic and electronic transport properties, leading to potential applications in the fields of photocatalysis and photovoltaics.[9−12]

In this work, we consider aqueous suspensions of gadolinium phosphate ($GdPO_4$) nanorods, of aspect ratio ∼12, that form a nematic liquid-crystalline phase at large concentrations. Due to the magnetic properties of gadolinium(III), we found that the nanorods are actually paramagnetic crystallites, which makes their suspensions very sensitive to an applied magnetic field. For example, the nematic phase is aligned in the weak fields created by small permanent magnets, and its nematic order parameter is unusually large ($S \approx 0.95$). Moreover, the isotropic phase becomes quite birefringent when submitted to the magnetic field. We investigated this unusual behavior of the $GdPO_4$ nanorod suspensions by combining synchrotron X-ray scattering, polarized-light microscopy, and magnetization measurements.

EXPERIMENTAL SECTION

Nanorod Synthesis and Functionalization. *Synthesis of $GdPO_4$ Nanorods.* A solution of 1.49 g (4 mmol) of $GdCl_3$ in 10 mL of water was heated up to 70 °C. A solution of NaH_2PO_4 (4 mmol in 10 mL) was then slowly added until the mixture turned milky; heating was then maintained for 4 h at 70 °C. The nanoparticle suspension was precipitated in acetone;

Received: April 3, 2012
Revised: May 23, 2012
Published: May 24, 2012

dx.doi.org/10.1021/jp303161a | J. Phys. Chem. B 2012, 116, 7590−7595

after centrifugation, the white solid obtained was redispersed in water as a stable colloidal suspension.

Grafting of the Bisphosphonate-PEG (BP-PEG) Derivative. 1-Hydroxy-2-(2-(2-(2-hydroxyethoxy)ethoxy)ethoxy)ethane-1,1-diyldiphosphonic acid was used to graft the surface of the nanorods in order to enhance the colloidal stability at high volume fractions. The synthesis of this compound is detailed in the Supporting Information.

Considering a total of 4 mmol of gadolinium, the Gd/bisphosphonate ratio was 3/1. A solution of 960 mg (1.33 mmol) of bisphosphonate-PEG was added to a 1 g suspension of $GdPO_4$ nanorods dispersed in 20 mL of water. The turbid mixture was heated up to 70 °C for 1 h. Purification was performed by dialysis. The suspension was then freeze-dried to give 900 mg of a white powder.

Concentrated solutions of different concentrations were obtained by slowly adding weighed amounts (400−700 mg) of modified $GdPO_4$ nanoparticles in 1 mL of water. The final pH of the solution was 5, and the zeta potential was +20 mV (see the Supporting Information for zeta potential versus pH measurements).

Transmission Electron Microscopy (TEM). The nanorod suspension was diluted by a factor of 100, and a drop was deposited on a copper grid covered with a holey carbon membrane to be examined by TEM (Topcon EM-002B, Akashi, Japan) with an operating voltage of 120 kV.

Sample Preparation for Optical Microscopy and Small-Angle X-ray Scattering. Samples of $GdPO_4$ nanorod colloidal suspensions were transferred into borosilicate cylindrical Lindemann capillary tubes (1 mm diameter, Mark-Rohrchen, Germany) for X-ray scattering experiments and into flat glass optical capillaries (optical path length ranging from 50 to 200 μm, VitroCom, NJ) for microscopic observations in polarized light. All capillaries were stored vertically after flame sealing.

Optical Microscopy. The samples were examined with an Olympus BX51 polarizing microscope, and their optical textures were photographed using an Olympus (Camedia C-3030) digital camera. Birefringence (Δn) measurements were performed under the microscope using a Berek (Olympus U-CBE) optical compensator.[13]

Magnetic Field Setup. In order to apply magnetic fields of variable intensities to $GdPO_4$ nanorod suspensions, we used a magnetic field setup based on two small permanent magnets. Samples held in glass capillaries were placed in between the two magnets, and the intensity of the magnetic field could easily be tuned between 0 and 1 T by changing the distance between the magnets. This setup was used both for optical microscopy and for synchrotron X-ray scattering experiments.

Small-Angle X-ray Scattering. Small-angle X-ray scattering (SAXS) experiments were performed at the SWING beamline of the SOLEIL synchrotron (Saint-Aubin, France). Measurements were carried out using a fixed energy of 12 keV and a sample to detector distance of 6.59 m. The typical accessible range of the scattering vector modulus q was 0.002−0.06 Å^{-1} ($q = 4\pi \sin\theta/\lambda$, where 2θ is the scattering angle and λ = 1.033 Å the wavelength). The incident X-ray beam transverse dimensions were approximately 600 × 200 μm^2 in the horizontal and vertical directions. 2D scattering patterns were recorded on an AVIEX 170170 CCD camera formed by four detectors. Exposure times were typically around 0.1 s. The curves of scattered intensity versus azimuthal angle were obtained by radial integration of the data along a narrow circular strip, at constant q, in the SAXS patterns.

Squid Measurements. The measurements of the magnetic moment as a function of field intensity were performed using a Quantum Design MPMS-5S Squid magnetometer. Small aliquots of aqueous dispersions were sealed in glass capillaries and introduced in the magnetometer. Measurements were performed at temperatures ranging from 238 to 298 K.

RESULTS AND DISCUSSION

$GdPO_4$ nanoparticles were synthesized by mixing two solutions of $GdCl_3$ and NaH_2PO_4 in water.[14] The mixture was heated at 70 °C for several hours. TEM images of the as-synthesized particles (Figure 1) show rod-like morphologies. On the basis

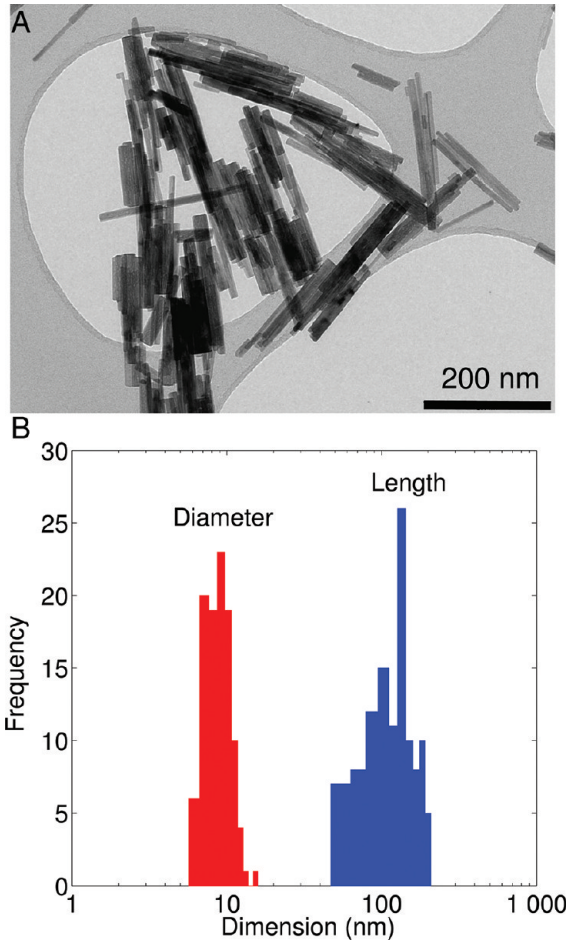

Figure 1. (A) Transmission electron microscopy image of $GdPO_4$ nanorods deposited on a microscopy grid and (B) histograms of particle dimensions.

of counting more than 100 particles, the average length is L = 125 nm with a standard deviation of 40 nm, whereas the average diameter is D = 9 nm with a standard deviation of 1.8 nm. Therefore, the aspect ratio of the bare nanorods is around $L/D \approx 14$.

After the synthesis, the surface of the particles was grafted with polyethylene-glycol chains functionalized with bisphosphonate units inducing strong short-range repulsions of the particles. The grafting efficiency was evidenced by FT-IR, and several bands, typical of the PEG units, were observed (Table 1).

dx.doi.org/10.1021/jp303161a | J. Phys. Chem. B 2012, 116, 7590−7595

Table 1. Assignments of the Main Vibrational Frequencies of Free and Grafted BP-PEG

free BP-PEG		BP-PEG grafted on $GdPO_4$	
freq. (cm^{-1})	assignments	freq. (cm^{-1})	assignments
2873	ν(C−H)	2865	ν(C−H)
1455, 1347	δ(C−H)	1458, 1351	δ(C−H)

This functionalization allows for dispersing of large amounts of particles in water. Samples containing as much as 700 mg of grafted particles per mL of water were prepared and did not show any trace of irreversible aggregation. TEM images of the grafted nanoparticles show that the chemical modification did not change the morphology of the $GdPO_4$ nanorods. However, considering a 1 nm thick organic layer, the aspect ratio of the grafted nanorods is ∼12.

Beyond a critical value of the nanorod concentration, around 460 mg/mL (volume fraction $\phi \approx 16\%$), a phase separation, occurs and a dense, concentrated phase sets at the bottom of the vial while a lighter, less turbid phase stands in equilibrium at the top of the vial. These biphasic samples were filled into flat glass capillaries and observed under a polarizing microscope (Figure 2a). While the dense phase at the bottom is highly birefringent, the dilute phase at the top is isotropic and therefore appears dark between crossed polarizers. The dense phase displays a threaded texture characteristic of a liquid-crystalline nematic phase (Figure 2b). These features indicate an isotropic to nematic phase transition, which is actually expected for colloidal suspensions of rod-like particles[2] and was confirmed by SAXS studies (see below). Moreover, the volume fraction at the transition (around 16%) agrees qualitatively with the predictions ($\phi \approx 27\%$ for the grafted nanoparticles) of the Onsager model.[2] Better agreement could probably be reached by incorporating electrostatic interactions in the model.[4] During the phase separation process, we observed the formation of droplets of the liquid-crystalline phase (also called tactoids; Figure 2c) in the isotropic phase. These droplets exhibit a typical "maltese cross" pattern due to the spatial variation of the nematic director within the droplet. The shape and director configurations have recently been studied in great detail in similar systems.[15,16] Altogether, these straightforward observations give direct evidence of the formation of a nematic phase at thermodynamic equilibrium, unaffected by gelation despite the large concentration. This latter parameter could not be increased much further, preventing the observation of more ordered mesophases due to the onset of particle aggregation. Besides, no effect of temperature on the stability of the nematic phase could be detected in the whole range of temperatures investigated (from room temperature to 95 °C). The athermal character of the isotropic to nematic transition is indeed a very common feature of mineral liquid crystals.[6] We also observed that the nematic phase has a strong tendency for homeotropic anchoring on the untreated flat glass walls of optical capillaries.

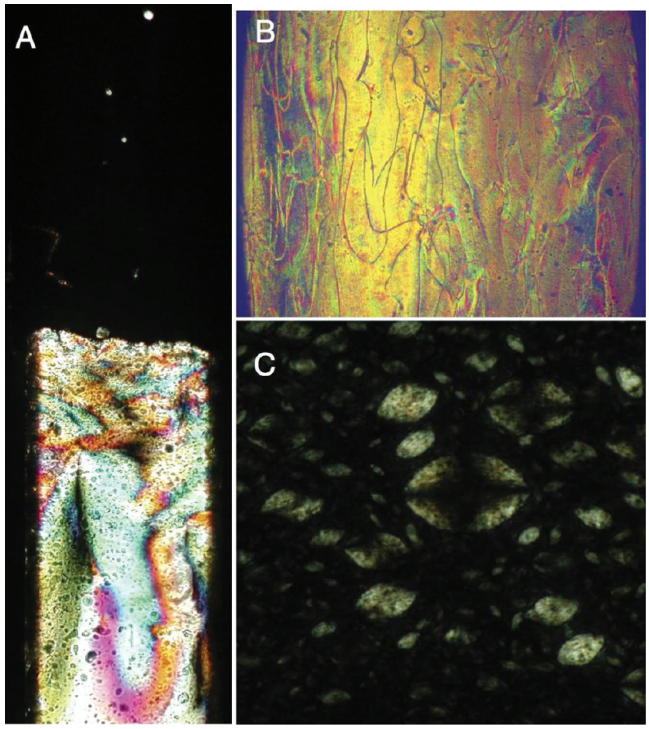

Figure 2. (A) Polarized optical microscopy of a glass capillary containing an isotropic/nematic biphasic sample. The birefringent nematic phase exhibits a typical threaded texture. (B) A typical threaded texture observed in the nematic phase. (C) Polarized light microscopy image of nematic tactoids growing in the isotropic phase of $GdPO_4$ nanorod suspensions.

With gadolinium being a paramagnetic atom, we investigated the effect of a magnetic field on the $GdPO_4$ nanorod suspension. Indeed, upon application of a rather small magnetic field (∼200 mT), the texture of the nematic phase completely disappeared, and a homogeneous birefringent nematic sample was obtained (Figure 3a). The measurement of the sample birefringence with an optical compensator gave $\Delta n = 4.4 \times 10^{-3}$, a value on the same order of magnitude as that of other mineral liquid crystals.[17] These observations strongly suggest that the nematic director aligns quite easily with respect to the direction of the magnetic field.

To confirm the structure and field-induced orientation of the liquid-crystalline phase, SAXS experiments were performed. This technique is particularly well-suited for this purpose because the high electronic density of the $GdPO_4$ particles ensures a high contrast with water. A SAXS pattern of the liquid-crystalline phase aligned in a magnetic field of 1 T is shown in Figure 3b. As expected, this pattern is typical of a nematic phase because it does not display any Bragg reflections or any "powder" sharp diffraction lines but only some diffuse scattering. This scattered intensity is strongly anisotropic and is concentrated in the direction perpendicular to the magnetic field, which shows that the nanorods align with their long axis parallel to the magnetic field. Moreover, the scattered intensity regularly decreases with scattering vector modulus, suggesting that there is very little local positional order.

To quantify the degree of orientation of the particles, we determined the value of the nematic order parameter S. This parameter can be derived from the dependence of the scattered intensity as a function of the azimuthal angle at a fixed scattering vector modulus, here $q = 0.1$ Å^{-1}. This intensity profile was fitted to a classical model describing the intensity scattered by an assembly of noninteracting nanorods with an orientational distribution of the Maier−Saupe form.[18,19] The experimental data and the fit are presented in Figure 4. The very large value obtained, $S \approx 0.95$ at $q = 0.1$ nm^{-1}, is quite uncommon and suggests a very strong coupling of the $GdPO_4$ nanorods with the magnetic field.

This unusual magnetic response is further underlined by the behavior of the isotropic phase submitted to a magnetic field.

dx.doi.org/10.1021/jp303161a | J. Phys. Chem. B 2012, 116, 7590−7595

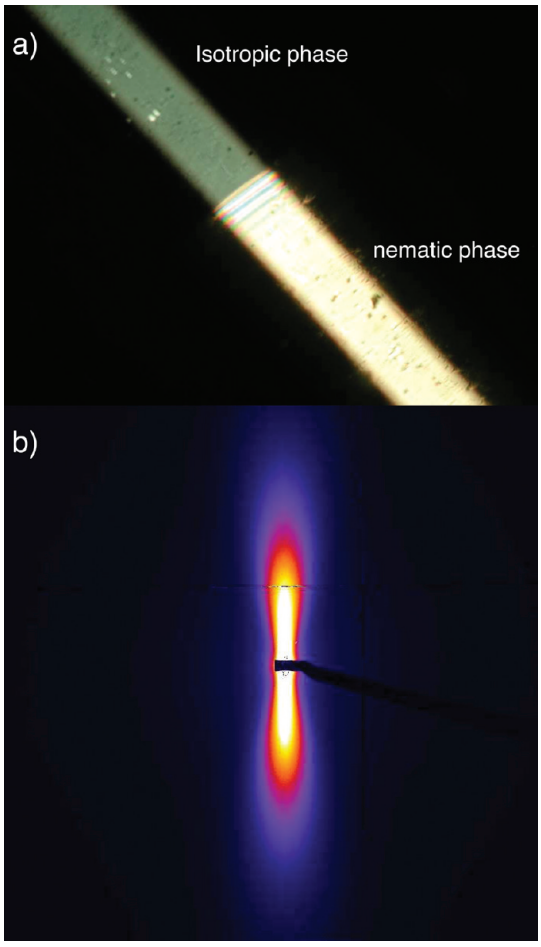

Figure 3. (a) Effect of a magnetic field on a biphasic sample similar to that shown in Figure 2A, as observed by polarized optical microscopy. (b) Small-angle X-ray scattering pattern of the nematic phase submitted to a magnetic field.

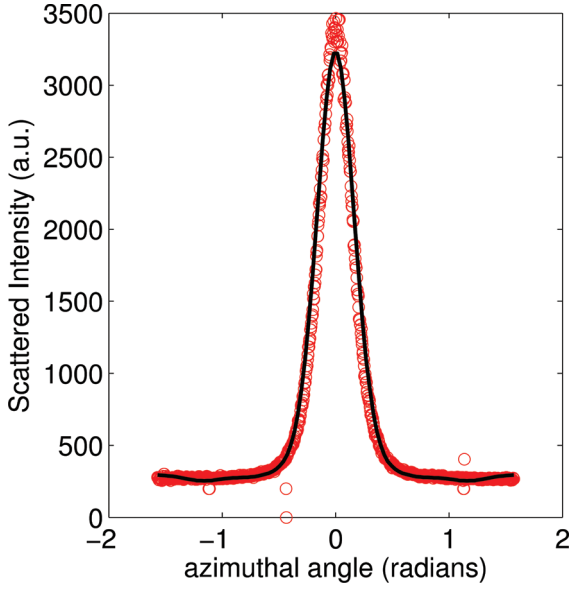

Figure 4. Dependence of the scattered intensity with the azimuthal angle, at q = 0.1 nm^{-1}, in the nematic phase aligned by a magnetic field.

Indeed, the isotropic phase acquires a fairly strong birefringence that gradually increases with field intensity (Figure 5) and

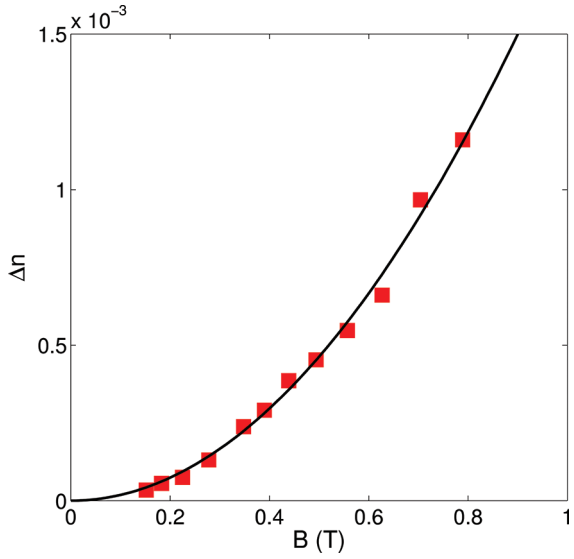

Figure 5. Dependence of the field-induced birefringence in the isotropic phase on magnetic field intensity. The solid line is a quadratic fit to the data.

immediately disappears when the field is suppressed. As expected, the field-induced birefringence follows a quadratic dependence with field intensity,[20] and no hint of saturation is detected up to the highest field (~0.8 T) that we applied. The coefficient of this quadratic dependence is $\Delta n/B^2 \approx 0.002$ T^{-2} for the isotropic phase at coexistence with the nematic phase. This value is about 5 orders of magnitude larger than that of the suspensions of rod-like viruses like the Tobacco Mosaic Virus and an order of magnitude larger than that of the suspensions of diamagnetic gibbsite platelets.[17,21] Therefore, the magnitude of the field-induced birefringence in isotropic suspensions of $GdPO_4$ nanorods is actually very large. On the other hand, it is 1 order of magnitude lower than that of the isotropic phase of the suspensions of goethite (α-FeOOH) nanorods that bear a permanent magnetic moment of 1000 μ_B per nanorod (where μ_B is the Bohr magneton).[20,22]

The origin of these uncommon magnetic effects in both the nematic and isotropic phases must lie in the magnetic properties of the nanorods. In order to obtain more insight in these properties, magnetization measurements in the isotropic phase were performed using a Squid magnetometer. The curve of the magnetization versus magnetic field intensity follows a straight line of positive slope (Figure 6), which means that the magnetic susceptibility is positive. Moreover, the straight line goes through the origin, even for field-cooled samples, which rules out the existence of any permanent magnetic moment. This is the typical behavior awaited for a paramagnetic material. The slope of this linear dependence is the magnetic susceptibility, which is 3×10^{-2} cm^3/mol at room temperature. The magnetic susceptibility followed a Curie–Weiss behavior in the temperature range investigated (238–298 K).

Another uncommon observation also confirms the paramagnetic nature of the $GdPO_4$ nanoparticles. When a sample of suspension is left for several days in a magnetic field gradient, the nanoparticles migrate to the regions of high field intensity,

dx.doi.org/10.1021/jp303161a | J. Phys. Chem. B 2012, 116, 7590–7595

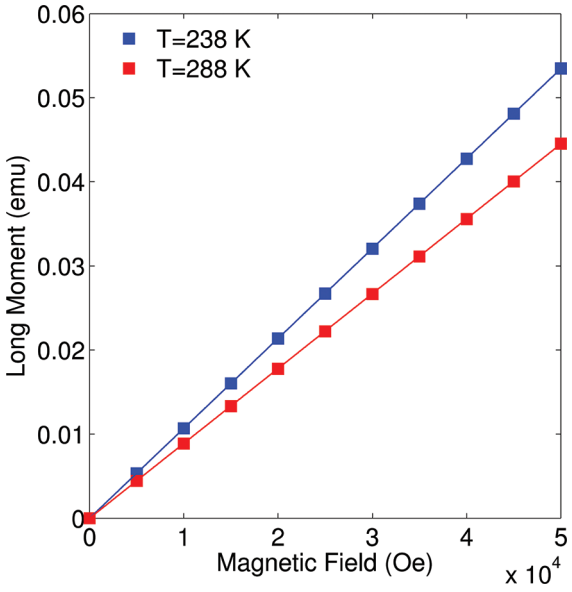

Figure 6. Dependence on the magnetic field intensity of the magnetization of an isotropic suspension of $GdPO_4$ nanorods.

as illustrated in Figure 7. The sample examined is biphasic with about equal amounts of isotropic phase (top) and nematic

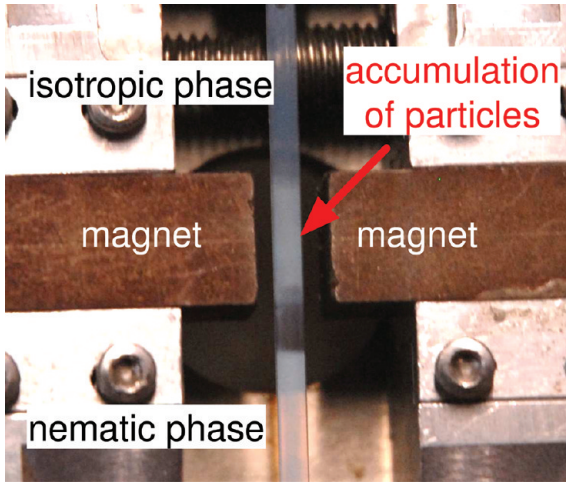

Figure 7. Photograph of a biphasic sample of an aqueous suspension of $GdPO_4$ nanorods left for several days in a 0.7 T magnetic field delivered onto the isotropic phase by permanent magnets (the two brown horizontal pieces on the image). In the vicinity of the magnets, the particles migrate to the region of high field intensity, and the region appears less transparent.

phase (bottom). Because the suspension turbidity increases with nanorod concentration, the nematic phase appears less transparent than the isotropic phase. Moreover, the part of the isotropic phase located in between the permanent magnets also appears more turbid, which shows that the nanoparticle concentration is much larger in this region where the phase becomes nematic. From this, we conclude that in the vicinity of the magnets, the nanorods have migrated to the regions of highest field, as expected for magnetic particles. When the magnetic field is suppressed, after a few days, the nanorod concentration relaxes to a uniform value in the whole isotropic phase of the sample.

Several examples of paramagnetic organometallic molecules that include lanthanide atoms in their structure and display liquid-crystalline phases as a function of temperature (thermotropic liquid crystals) have already been reported.[23,24] These compounds show magnetic susceptibilities in the range of $1-5 \times 10^{-2}$ cm^3/mol, which is comparable to the value reported in this work. Paramagnetic liquid crystals have recently raised interest because they are, in principle, easier to align than their diamagnetic counterparts. They could then find applications where magnetic field alignment would be preferred to usual electric field alignment processes because larger samples can be used and charge injection effects can be avoided. In this context, colloidal nematic suspensions of $GdPO_4$ nanorods are much easier to synthesize than organometallic thermotropic liquid crystals, and they are much less sensitive to temperature. These two features could make them a very attractive alternative in the future for such applications.

■ ASSOCIATED CONTENT

Supporting Information

Synthesis of the ligand, diffraction pattern, and zeta potential measurements of the nanorods. This material is available free of charge via the Internet at http://pubs.acs.org.

■ AUTHOR INFORMATION

Corresponding Author

*E-mail: benjamin.abecassis@u-psud.fr.

Notes

The authors declare no competing financial interest.

■ ACKNOWLEDGMENTS

We thank the Soleil Synchrotron (Saint-Aubin, France) for the award of beamtime 99110058 and Florian Meneau for help during the SAXS experiments. We also thank Frédéric Chaput and Marc Lecouvey for very helpful discussions.

■ REFERENCES

(1) De Gennes, P. G. *The Physics of Liquid Crystals*; Clarendon Press: Oxford, U.K., 1974.
(2) Onsager, L. *Ann. N.Y. Acad. Sci.* **1949**, *51*, 627−659.
(3) Bolhuis, P.; Frenkel, D. *J. Chem. Phys.* **1997**, *106*, 666−687.
(4) Vroege, G. J.; Lekkerkerker, H. N. W. *Rep. Prog. Phys.* **1992**, *55*, 1241−1309.
(5) Dogic, Z.; Fraden, S. *Curr. Opin. Colloid Interface Sci.* **2006**, *11*, 47−55.
(6) Davidson, P.; Gabriel, J. C. P. *Curr. Opin. Colloid Interface Sci.* **2005**, *9*, 377−383.
(7) Tombolato, F.; Ferrarini, A.; Grelet, E. *Phys. Rev. Lett.* **2006**, *96*, 258302.
(8) van der Kooij, F. M.; van der Beek, D.; Lekkerkerker, H. N. W. *J. Phys. Chem. B* **2001**, *105*, 1696−1700.
(9) Miyamoto, N.; Yamada, Y.; Koizumi, S.; Nakato, T. *Angew. Chem., Int. Ed.* **2007**, *46*, 4123−4127.
(10) Dessombz, A.; Chiche, D.; Davidson, P.; Panine, P.; Chaneac, C.; Jolivet, J. P. *J. Am. Chem. Soc.* **2007**, *129*, 5904−5909.
(11) Zhang, S. J.; Pelligra, C. I.; Keskar, G.; Majewski, P. W.; Ren, F.; Pfefferle, L. D.; Osuji, C. O. *ACS Nano* **2011**, *5*, 8357−8364.
(12) Meuer, S.; Oberle, P.; Theato, P.; Tremel, W.; Zentel, R. *Adv. Mater.* **2007**, *19*, 2073−2078.
(13) Born, M.; Wolf, E. *Principles of Optics: Electromagnetic Theory of Propagation, Interference and Diffraction of Light*, 7th ed.; Cambridge University Press: New York, 1999.
(14) Wang, X. J.; Gao, M. Y. *J. Mater. Chem.* **2006**, *16*, 1360−1365.
(15) Verhoeff, A. A.; Bakelaar, I. A.; Otten, R. H. J.; van der Schoot, P.; Lekkerkerker, H. N. W. *Langmuir* **2011**, *27*, 116−125.

(16) Kaznacheev, A. V.; Bogdanov, M. M.; Sonin, A. S. *J. Exp. Theor. Phys.* **2003**, *97*, 1159−1167.
(17) van der Beek, D.; Petukhov, A. V.; Davidson, P.; Ferre, J.; Jamet, J. P.; Wensink, H. H.; Vroege, G. J.; Bras, W.; Lekkerkerker, H. N. W. *Phys. Rev. E* **2006**, *73*, 041402.
(18) Hayter, J. B.; Penfold, J. *J. Phys. Chem.* **1984**, *88*, 4589−4593.
(19) Li, M. H.; Brulet, A.; Davidson, P.; Keller, P.; Cotton, J. P. *Phys. Rev. Lett.* **1993**, *70*, 2297.
(20) Lemaire, B. J.; Davidson, P.; Ferre, J.; Jamet, J. P.; Petermann, D.; Panine, P.; Dozov, I.; Jolivet, J. P. *Eur. Phys. J. E* **2004**, *13*, 291−308.
(21) Fraden, S.; Maret, G.; Caspar, D. L. D. *Phys. Rev. E* **1993**, *48*, 2816−2837.
(22) Lemaire, B. J.; Davidson, P.; Ferre, J.; Jamet, J. P.; Panine, P.; Dozov, I.; Jolivet, J. P. *Phys. Rev. Lett.* **2002**, *88*, 125507.
(23) Galyametdinov, Y. G.; Haase, W.; Goderis, B.; Moors, D.; Driesen, K.; Van Deun, R.; Binnemans, K. *J. Phys. Chem. B* **2007**, *111*, 13881−13885.
(24) Galyametdinov, Y. G.; Haase, W.; Malykhina, L.; Prosvirin, A.; Bikchantaev, I.; Rakhmatullin, A.; Binnemans, K. *Chem.—Eur. J.* **2001**, *7*, 99−105.